Lab on a Chip

CrossMark
click for updates

In vitro evaluation and *in vivo* demonstration of a biomimetic, hemocompatible, microfluidic artificial lung

K. M. Kovach,[a] M. A. LaBarbera,[b] M. C. Moyer,[cd] B. L. Cmolik,[e] E. van Lunteren,[c] A. Sen Gupta,[f] J. R. Capadona[af] and J. A. Potkay*[abgh]

Despite the promising potential of microfluidic artificial lungs, current designs suffer from short functional lifetimes due to surface chemistry and blood flow patterns that act to reduce hemocompatibility. Here, we present the first microfluidic artificial lung featuring a hemocompatible surface coating and a biomimetic blood path. The polyethylene-glycol (PEG) coated microfluidic lung exhibited a significantly improved *in vitro* lifetime compared to uncoated controls as well as consistent and significantly improved gas exchange over the entire testing period. Enabled by our hemocompatible PEG coating, we additionally describe the first extended (3 h) *in vivo* demonstration of a microfluidic artificial lung.

Introduction

Artificial lungs, or blood oxygenators, have been used clinically since the 1970's.[1] These devices act to exchange oxygen and carbon dioxide from the blood, supporting the function of a patient's natural lungs in cases of disease or trauma as well as during cardiopulmonary bypass procedures. Most current artificial lungs are comprised of bundles of porous hollow fibers, across which gases are exchanged *via* diffusion between oxygen flowing through the fiber lumens and blood flowing across the outside of the fibers.

Though effective in acute (days) settings, this technology suffers from a number of drawbacks that precludes truly portable systems and prevents their use in more chronic applications. First, current devices exhibit poor hemocompatibility in the long term, due in part to large priming volumes, surface hydrophobicity, and a tortuous blood flow path across

the hollow fibers.[2–4] These factors work together to accelerate the coagulatory response of the blood, resulting in premature device failure as well as thromboembolisms which can be returned to the bloodstream of the patient. Other drawbacks of the hollow fiber design include: 1) fiber porosity which results in plasma leakage into the fiber pores and decreased functionality, and 2) large blood side gas diffusion distances, decreasing efficiency and necessitating the use of pure oxygen as the supply gas.[2,4,5]

Microfluidic or microchannel-based designs aim to increase the efficiency and lifetime of artificial lungs by addressing many of these issues.[2–8] Microfluidic lungs operate similarly in concept to hollow fiber devices, in that they separate gas and blood flow paths with a membrane across which gas exchange occurs. However, by utilizing micron scale feature sizes on the order of those found in the natural lung, microchannel devices are able to achieve very high surface area to volume ratios, thus decreasing diffusion distances and priming volumes and increasing gas transfer efficiency.[4,5,9] Polymer microfabrication techniques such as soft lithography also allow for the microchannel networks to be custom built in almost any two-dimensional configuration.[10] These custom flow networks can be designed to closely mimic the physiologic environment (in terms of pressure and shear stress) of the natural lung and allow designs that can operate with natural vascular pressures.[4,8] Finally, the use of thin, nonporous polymer membranes can increase gas transfer efficiency while eliminating the threat of plasma leakage. Despite these advantages, microfluidic devices constructed from poly(dimethylsiloxane) (PDMS) still suffer from premature failure due in large part to the accelerated intrinsic coagulation response on the hydrophobic

[a] *Advanced Platform Technology Center (APT Center), Louis Stokes Cleveland VA Medical Center, Cleveland, OH 44106, USA*
[b] *Department of Electrical Engineering and Computer Science, Case Western Reserve University, Cleveland, OH 44106, USA*
[c] *Pulmonary, Critical Care, and Sleep Division, Department of Medicine, Louis Stokes Cleveland VA Medical Center, Cleveland, OH 44106, USA*
[d] *Pulmonary, Critical Care, and Sleep Division, Department of Medicine, Case Western Reserve University, Cleveland, OH 44106, USA*
[e] *Surgical Service, Louis Stokes Cleveland VA Medical Center, Cleveland, OH 44106, USA*
[f] *Department of Biomedical Engineering, Case Western Reserve University, Cleveland, OH 44106, USA*
[g] *VA Ann Arbor Healthcare System, Ann Arbor, MI 48105, USA*
[h] *Department of Surgery, University of Michigan, Ann Arbor, MI 48109, USA. E-mail: jpotkay@umich.edu*

material surface.[11] To combat this, researchers have investigated methods to improve the hemocompatibility of PDMS microchannels.[12–15]

Our group has developed a PDMS microchannel artificial lung that achieves a higher gas transfer efficiency than any artificial lung to date.[5] In tandem, we have also developed a method of applying a durable, hemocompatible poly(ethylene glycol) (PEG) coating to the surfaces of intact microchannels.[12] Although achieving excellent gas exchange efficiency, our previous microfluidic design had two main drawbacks: 1) it had poor hemocompatibility due to lack of a surface functionalization; and, 2) its microfluidic channel structure had inefficiencies that created areas of high and low shear stress and inefficient blood delivery. In this work, we describe the design and fabrication of a new small-scale microfluidic artificial lung that is the first such device with a biomimetic flow path and a hemocompatible coating. We discuss these interrelated components as they relate to the successful design of a complete microfluidic artificial lung and our microfabrication process which we use to simultaneously create the microfluidic network and provide functionalization of the blood contacting surfaces. Our microfluidic lung was tested under whole blood flow *in vitro* and evaluated in terms of functional lifetime and gas exchange efficiency. Finally, we describe the first extended demonstration of a microfluidic artificial lung in an animal model, enabled by the applied hemocompatible coating.

Materials and methods

Materials

For silicon wafer mold fabrication, SU-8 2035 permanent epoxy negative photoresist and SU-8 developer were purchased from MicroChem (Newton, MA), and 2-isopropanol was purchased from Sigma Aldrich (St. Louis, MO). For device fabrication and testing, Sylgard 184 silicone elastomer base and curing agent were obtained from Dow Corning (Midland, MI). 2-[methoxy(polyethyleneoxy)propyl]trimethoxysilane (PEG-silane), tech-90, 6–9 C_2H_4O groups was purchased from Gelest (Morrisville, PA). Acetone, 99.8%, extra dry was obtained from Acros Organics (Geel, Belgium). Dulbecco's phosphate-buffered saline (PBS) was purchased from Life Technologies (Grand Island, NY). CPD-anticoagulated (14% v/v) adult bovine whole blood was obtained from LAMPIRE Biological Laboratories (Pipersville, PA) and male Sprague–Dawley rats (326–350 g) were purchased from Charles River (Wilmington, MA). Heparin sodium injection, USP (1000 U mL^{-1}) was obtained from Hospira.

Microfluidic lung design

Similar to previous work,[5] the device was designed to have a three-layer structure (air layer/membrane/blood layer) in PDMS. As blood flows through the device on the blood side, oxygen diffuses from the air side, through the non-porous membrane, and into the blood enriching it. Carbon dioxide diffuses in the opposite direction and is removed from blood

by the microfluidic lung. Highly-efficient gas exchange can be achieved due to the micron-scale diffusion distances and large surface-area-to-volume ratio.[4,5] Overall, this microfluidic artificial lung was designed to: 1) maximize gas exchange efficiency; 2) enable operation with natural pressures; and, 3) be biomimetic to provide a natural environment for blood cells and platelets. In pursuit of these goals, the blood flow network was divided into a blood distribution network and gas exchange network (artificial capillaries). Similar to in the native lung,[16] the blood distribution network was designed to efficiently deliver blood to the artificial capillaries with minimal work (small pressure drop) and the artificial capillaries were designed to maximize gas exchange. More details of the optimization of each design parameter are described below.

Gas exchange. Gas exchange in the artificial capillaries was modeled using a previously-developed equation:[4,9]

$$Q_R = \frac{A}{S_{B,O_2} \cdot R_{D,O_2} \cdot \ln\left(\dfrac{P_{O_2 B,i} - P_{O_2 G}}{P_{O_2 B,o} - P_{O_2 G}}\right)} \quad (1)$$

where Q_R is the rated blood flow of the artificial capillaries and is defined as the maximum blood flow rate at which an inlet blood saturation of 70% can be oxygenated to an outlet oxygen saturation of 95%.[17] Rated flow is thus a simple and direct measure of the both the gas exchange and blood flow capacity of an artificial lung. In eqn (1), A is the capillary area available for gas exchange, S_{B,O_2} is the average effective solubility of oxygen in blood, $P_{O_2 B,i}$ and $P_{O_2 B,o}$ are the partial pressures of oxygen in blood at the inlet and outlet of the capillaries, respectively, $P_{O_2 G}$ is the partial pressure of oxygen in the supply gas, and R_{D,O_2} is the resistance to diffusion of oxygen as given in eqn (2).

$$R_{D,O_2} = \frac{\delta_M}{P_{M,O_2}} + \frac{H/2}{S_{B,O_2} \cdot D_{B,O_2}} \quad (2)$$

In eqn (2), δ_M is the membrane thickness, P_{M,O_2} is the permeability of the membrane to oxygen, H is the artificial capillary height, and D_{B,O_2} is the effective diffusivity of oxygen in blood. For normal human blood, as defined by the FDA Guidance for Cardiopulmonary Bypass Oxygenators 510(k) Submissions,[18] S_{B,O_2} and D_{B,O_2} can be estimated to be 7.9 × 10^{-4} mL-O$_2$ mL-blood^{-1} mmHg^{-1} and 1.4 × 10^{-6} cm^2 s^{-1}, respectively.[9] Using the Hill equation,[19] an inlet blood saturation of 70% corresponds to a $P_{O_2 B,i}$ of 36.4 mmHg and an outlet blood saturation of 95% corresponds to a $P_{O_2 B,o}$ of 79.2 mmHg.[4] The theoretical model (eqn (1) and (2)) predicts a maximum rated flow for minimum artificial capillary height (H) and minimum membrane thickness (δ_M). An artificial capillary height of 10 μm was thus chosen to maximize gas exchange and permit passage of all components of blood. A membrane thickness of 15 μm was chosen based on our previous experience[5] to ensure a large gas exchange, a defect-free membrane, and adequate mechanical strength and durability.

Biomimetic blood flow path. The blood distribution network was designed to be biomimetic and to maximize area efficiency. For all portions of the design except the edge regions, a symmetric trifurcating network was implemented where two identical daughter vessels branch off from a parent vessel (Fig. 1). The relationship between parent and daughter channels in regard to branching angles and channel radii were designed using Murray's law.[16,20,21] In the equations below, two equal daughter channels (radii r_1) branch off from the parent channel (radius r_0) and the parent continues on its course with a reduced radius, r_2.

$$r_0^3 = 2r_1^3 + r_2^3 \qquad (3)$$

$$\cos(\alpha) = \frac{r_0^2 - \left(r_0^3 + 2r_1^3\right)^{2/3}}{2r_1^2} \qquad (4)$$

In eqn (4), α is the branching angle at which the daughter channels (radii r_1) branch off from the parent channel. Since the channels have a rectangular cross-section, the hydraulic radii of the channels were determined as $r_H = H \cdot W/(H + W)$, where H and W are the channel height and width, respectively. Where necessary, the change in the radius of the parent vessel was linearized and the branching angle was averaged among multiple daughter vessels in order to provide an area efficient layout.

Pressure drop. Pressure drop (ΔP) in the rectangular channels was calculated using:

$$\Delta P = \frac{12\mu \cdot L}{H \cdot W^3 \cdot \left(1 - \dfrac{0.63 \cdot H}{W}\right)} Q \qquad (5)$$

In eqn (5), μ is blood viscosity (~2 cP (ref. 5)), L is the channel length, and Q is the blood flow through the channel. The difference between the mean arterial and venous pressures in a normal adult is approximately 80 mmHg.[22] The

pressure drop between the pulmonary artery and left atrium is approximately 10 mmHg.[22] These two values thus provide upper and lower bounds for the total pressure drop of the device at its maximum (rated) flow.

Shear stress. Shear stress was estimated as $\tau = \mu \cdot v \cdot H^{-1}$, where τ is shear stress and v is average flow velocity in the channel. In the human vascular system, shear stress ranges between 10 and 70 dyn cm^{-2} in arteries and between 1 and 6 dyn cm^{-2} in veins.[23] The human body naturally compensates to maintain a mean arterial shear stress between 15 and 20 dyn cm^{-1}.[23] These values provided upper and lower bounds for the shear stress in our blood flow network.

Air side. The air side of the lung device was designed to allow for an even flow of the sweep gas across the entire network, while maximizing the total surface area available for gas exchange with the blood side capillaries. In order to ensure mechanical durability, 20% of the air network surface area is comprised of identical, evenly spaced, rectangular "posts" that form the bond to the membrane, leaving 80% of the total area available for blood gas exchange. The air side channel height was chosen so that the pressure drop was minimal (<5 mmHg) at all target air flow rates (up to 20 mL min^{-1}).

Fabrication and assembly

Lung devices were fabricated and assembled according to previously described microfabrication methods.[5,12] Briefly, Sylgard 184 silicone polymer (PDMS) was mixed and poured over Si wafer master molds for the blood and air sides of the device. A small amount of polymer was also poured onto a 4.5" diameter acrylic circle and spin-coated to 15 μm (5500 rpm, 60 s). These device components were then cured at 80 °C for 1 h. Once cured, the device halves were peeled off of the Si wafers, cut to shape, and inlet/outlet (I/O) holes were punched out using a biopsy punch. Short sections of tubing were then plasma bonded to the I/O holes of the blood side of the device. To begin device assembly, the air side and membrane were plasma treated and brought into contact to form an irreversible bond.[24] The air side was then carefully peeled off of the acrylic circle, leaving the thin membrane bonded across the entire surface. To complete the device, the air side and membrane section was bonded to the blood side of the device in the same manner. Immediately following bonding, the PEG coating was applied to the blood side of the device as previously described.[12] Finally, tubing sections were sealed to the I/O ports of the air side using Sylgard 184 and allowed to cure completely.

In vitro testing

The microfluidic lung devices were characterized in terms of: a) fluidic pressure *vs.* flow relationship; b) the effects of blood and sweep gas flow rates on gas exchange performance; and, c) device lifetime under whole blood flow, as previously described,[12] with minor alterations. CPD-anticoagulated bovine blood was stored upon receipt in a refrigerator
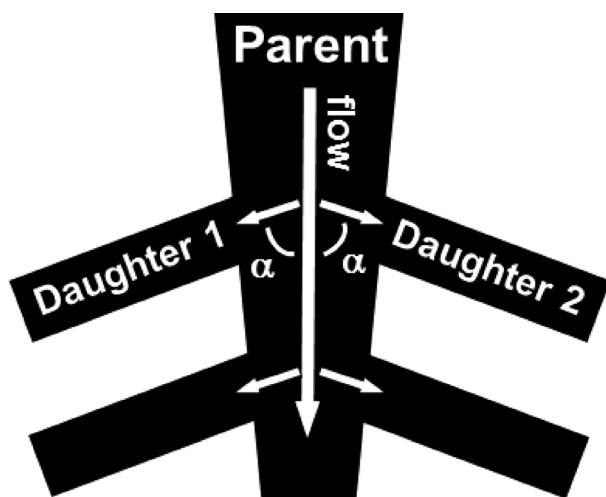

Fig. 1 Schematic of parent/daughter channel branching.

overnight prior to testing in order to equilibrate the oxygen saturation (S_{O_2}) and oxygen and carbon dioxide partial pressures (p_{O_2} and p_{CO_2}) to normal venous levels.[18] While priming the flow circuit with PBS, the blood was warmed to 37 °C in a shaking water bath and gently agitated to ensure constant and even mixing. Once equilibrated to temperature, the blood was pumped into the circuit tubing, through the devices, and out into a waste reservoir in an open loop configuration. For the characterization experiments, only one device was tested at a time. In the device lifetime experiment, two devices (one uncoated and one PEG-coated) were tested simultaneously using the same blood reservoir in order to facilitate direct comparison of the resulting data. The blood flow rate was set at 0.5 mL min^{-1} (slightly above the rated flow) so that changes in blood saturation would be more apparent. No blood filter was used. Devices were fed with compressed air regulated to the desired level *via* an Omega FMA5502 mass flow controller (Stamford, CT). The S_{O_2}, p_{O_2}, and p_{CO_2} in the blood as well as other parameters were measured from the blood reservoir and device outlets using an iStat handheld blood analyzer (Abbott, Abbott Park, IL) and CG8+ cartridges throughout the experiment.

The fluidic pressure drop across a device was measured with a Honeywell 26PCCFA6D pressure sensor as previously described.[12] The inlet air pressure (Honeywell 26PCCFA6D) and outlet air flow (Honeywell AWM3100V gas flow sensor) were additionally measured throughout the experiments. For the characterization experiments, 1) the air flow rate was held constant while fluidic pressure and gas exchange were measured with varying blood flow rates, and 2) the blood flow rate was held constant while the gas exchange was measured over a range of air flow rates. Five minutes of equilibration time were given between sequential measurements for these characterization experiments, with the test ending after the final measurement was taken. The lifetime experiment was run until either the initial pressure drop across a device doubled in magnitude, or four hours elapsed. The experiment was not continued past four hours in order to ensure the integrity and functionality of the blood cells and proteins. The time until a doubling of the initial pressure drop was defined as the lifetime or time until failure for a device. Doubling time was chosen as an arbitrary threshold used in order to easily compare devices. Following the lifetime experiment, the devices were washed with PBS and imaged to observe surface-bound clots.

In vivo testing

An adult male Sprague–Dawley rat was anesthetized with 1–2% isoflurane gas and maintained under anesthesia on a heating pad for the duration of the experiment. The rat's vital signs were monitored using a MouseOx Plus pulse oximeter (Starr Life Sciences, Oakmont, PA) with a foot pad sensor. Prior to the experiment, the lung device and external tubing were primed with 400 U kg^{-1} of 1000 U mL^{-1} heparin in PBS in order to prevent clotting in the tubing circuit. Once anesthetized, the

rat was given a 400 U kg^{-1} dose of heparin *via* tail vein injection five minutes prior to the following surgical procedures. In this experiment run in parallel with the *in vitro* studies, a previously characterized lung device[5] with an applied PEG coating was used. To connect the device, the rat's femoral artery and vein were exposed, cannulated with short sections of PE-50 polyethylene tubing, and gently clamped to temporarily impede blood flow. The tubing was then connected to the inlet and outlet of the lung device and the clamps were removed from the femoral vessels allowing blood to begin flowing through the extracorporeal tubing circuit. In this configuration, the blood was pumped by the natural pressure of the femoral artery into the lung device and returned to the venous circulation through the femoral vein. Thus, instead of operating as a true artificial lung, here the device acts more as an arteriovenous CO_2 removal system (AVCO2-R) removing CO_2 from the arterial circulation.[25] In this preliminary work, only one rat was tested.

Throughout the experiment, the fluidic pressure drop across the lung device as well as the partial pressures of O_2 and CO_2 in the blood at the device I/O were measured over the three hour duration as described in the previous *in vitro* experiments. Following the experiment, the rat was sacrificed. All procedures were performed in accordance with institutional IACUC and IRB approved protocols.

Statistics

Three lung devices for both the PEG-coated and uncoated groups were tested for the blood lifetime experiment. Results were analyzed in Microsoft Excel using a Student's *t*-test and ANOVA. Plotted data for p_{CO_2}, S_{O_2}, and blood side pressure drop are presented as mean values ± standard deviation.

Results

Device design

The finished blood flow path layout is displayed in Fig. 2 and 3 depicts an assembled artificial lung with dyed water flowing through both the blood and air side of the device. Blood enters through large, 200 μm-high microfluidic channels and then branches into smaller 60 μm-tall channels (branching angle of 81°), then finally into the 10 μm-high artificial capillaries (branching angle of 83°). In total there are 8897 artificial capillaries, each with a width of 60 μm and length of 370 μm. These dimensions result in a predicted rated flow of 0.4 mL min^{-1} for the device (eqn (1)), a pressure drop of 0.9 mmHg (eqn (5)) and shear stress of 2.5 dyn cm^{-2} for the artificial capillaries. The width of the 60 μm-tall channels varies from 300 to 120 μm as an intentional design feature, a consequence of Murray's law. The vertical segments of the 200 μm-tall channels vary in width from 4000 to 600 μm and the width of the 200 μm-tall horizontal segments varies from 9700 to 4200 μm. The predicted flow resistance of the entire blood flow network is 5.9 mmHg mL^{-1} min, resulting in a predicted pressure drop of 2.4 mmHg at the device's rated flow.
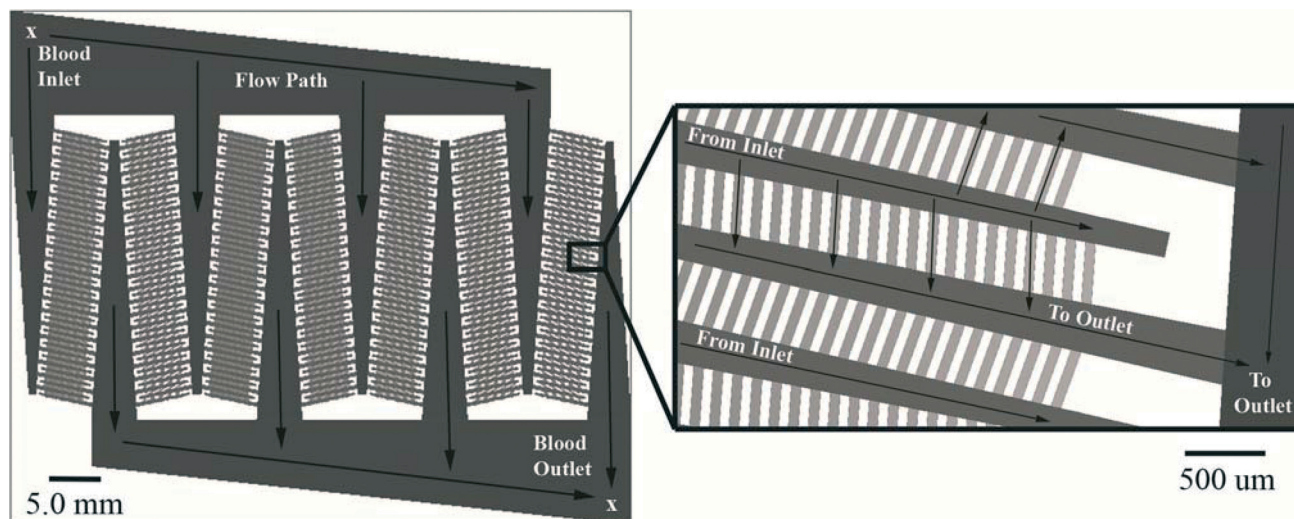
Fig. 2 CAD drawing of the device's blood channel network and capillary branches (right inset).

Pressure and gas exchange characterization

Fig. 4 displays the pressure-flow relationship in a PEG-coated and uncoated device as whole bovine blood is pumped through each device. Here, the air flow rate through the devices was held constant at 5 mL min^{-1}. As expected, both devices exhibited a linear pressure-flow relationship. Fig. 5 highlights the effects of blood and air flow rates on the S_{O_2} of the blood exiting the lung device. S_{O_2} begins to decrease quickly as the blood flow rate increases past the device's rated flow, but is unaffected by air flow rate. Similarly, the effect of air flow rate on blood p_{CO_2} is shown in Fig. 6, again observed to have negligible effects. In these initial characterization experiments, data points were gathered at 5 minute intervals and the tests were ended after the last data point was collected. Only PEG-coated devices were used in Fig. 5 and 6 to highlight the performance trends of the optimized design.

In vitro performance

Before each lifetime experiment, the bovine blood was measured to have baseline values of pH = 7.011 ± 0.05,

hematocrit = 24.3 ± 4.5%, and hemoglobin = 8.3 ± 1.5 g dL^{-1}. Throughout the duration of the test, the S_{O_2} of the blood was measured at the outlet of the lung devices and compared to the original oxygen saturation of the blood in the reservoir (Fig. 7). Both the uncoated and PEG-coated devices significantly increase the S_{O_2} of the blood at all time points compared to blood in the reservoir. S_{O_2} values for the PEG-coated lung device are not statistically different over the four hours, while those of the uncoated device significantly decrease compared to the coated group between 0–60 min.

The fluidic pressure drop across the tested devices was also measured (Fig. 8). At all time points where the full $n = 3$ devices could be compared, the pressure across the uncoated artificial lung was significantly greater than the PEG-coated device (with the exception of 10 min). One of the three uncoated devices that was tested exhibited a higher initial pressure drop than the other two, but stabilized over time to a similar level thus increasing the calculated standard deviation at early time points. These differences in initial pressure drop (as well as device priming) may be related to innate compositional and viscosity differences between donor blood batches. The lifetime (time until pressure doubling) of the
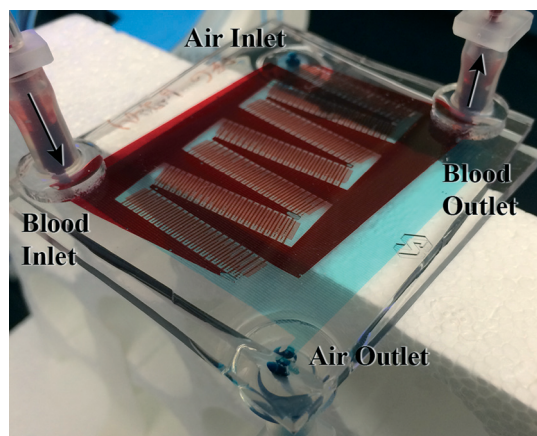

Fig. 3 Fully constructed lung device operating with dyed water flowing through both the blood (red) and air side (blue) for visualization.
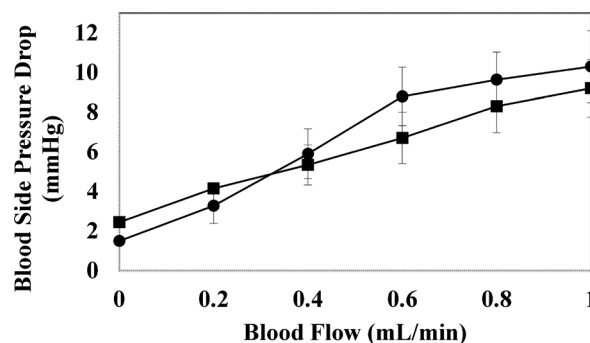

Fig. 4 Relationship between blood flow rate and fluidic pressure drop for PEG-coated (■) and uncoated (●) lung devices ($n = 1$). Air flow was held constant at 5 mL min^{-1}.
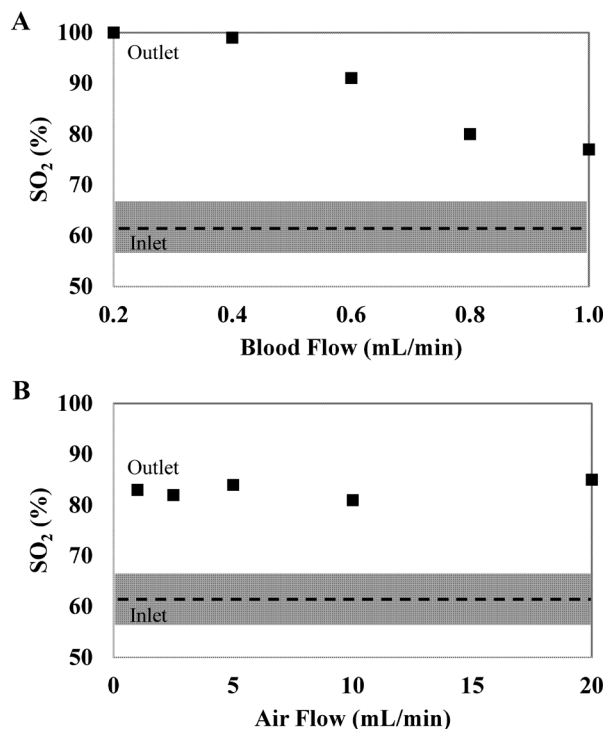
A

B

Fig. 5 S_{O_2} of blood at the lung device outlet as a function of blood flow rate with air flow held constant at 5 mL min^{-1} (A) and air flow rate with blood flow held constant at 0.5 mL min^{-1} (B), $n = 1$. An average ± standard deviation from the beginning and end of the experiment of the blood S_{O_2} entering the device is denoted by the dashed line (----) and gray bar.
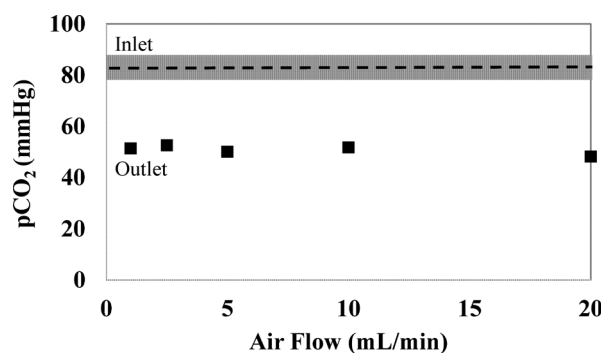

Fig. 6 Partial pressure of carbon dioxide at the artificial lung outlet as a function of air flow rate ($n = 1$). Blood flow was held constant at 5 mL min^{-1}. An average ± standard deviation from the beginning and end of the experiment of the blood p_{CO_2} entering the lung is denoted by the dashed line (----) and gray bar.

uncoated lung devices was 110.0 ± 37.7 min as compared to all PEG devices completing the full 240 minute experiment without failing. Because the variation in pressure measurements for the coated device was not statistically significant over 240 min, it is not possible to predict a failure time for this group. Fig. 9 contains representative macro and microscopic images of PBS-washed artificial lungs following the lifetime experiment, highlighting the differences in clotting within the microchannel networks of each device.
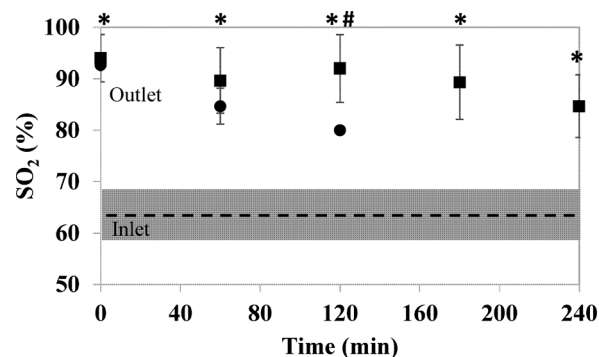

Fig. 7 S_{O_2} of blood exiting PEG-coated (■) and uncoated (●) artificial lungs as compared to the original blood entering the devices. Both blood and air flow rates were held constant at 5 mL min^{-1}. S_{O_2} of the original blood is presented as an average ± standard deviation from the beginning and end of the experiments and is denoted by the dashed line (----) and gray bar. Data points are the mean ± std. deviation ($n = 3$). * $p < 0.05$ comparing both lung devices to the original blood. # denotes that only one uncoated device reached this time point.

In vivo performance

As in the *in vitro* experiments, the fluidic pressure drop across the rat-connected, PEG-coated lung device was measured over time. Once the device was fully filled with blood and the pressure equilibrated at approximately 30 min, the pressure was observed to remain relatively stable until the end of the three hour experiment (Fig. 10).

Simultaneously, blood was sampled from the inlet and outlet of the lung device and the partial pressures of O_2 and CO_2 were measured (Fig. 11). The artificial lung's ability to exchange oxygen and carbon dioxide from the blood is apparent in the large reduction in p_{O_2} and p_{CO_2} after moving through the device at all time points. Oxygen is being removed from the blood due to the experimental setup where the rat is ventilated with pure (100%) O_2 under anesthesia, while the lung device is being fed with compressed air (21% O_2).
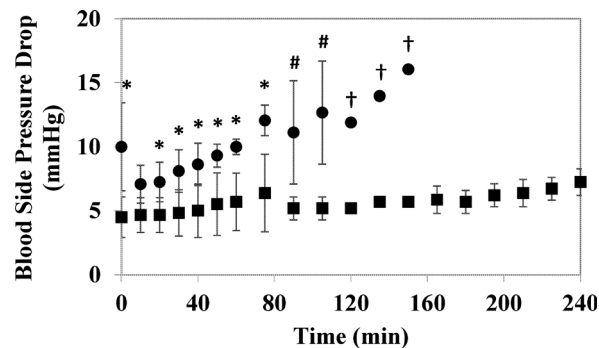

Fig. 8 Blood side pressure measurements over time for PEG-coated (■) and uncoated (●) lung devices. Blood and air flow rates were held constant at 0.5 and 5 ml min^{-1}, respectively. Data are the mean ± std. deviation ($n = 3$). * $p < 0.05$. # and † denote that only two and one uncoated devices reached these time points, respectively.
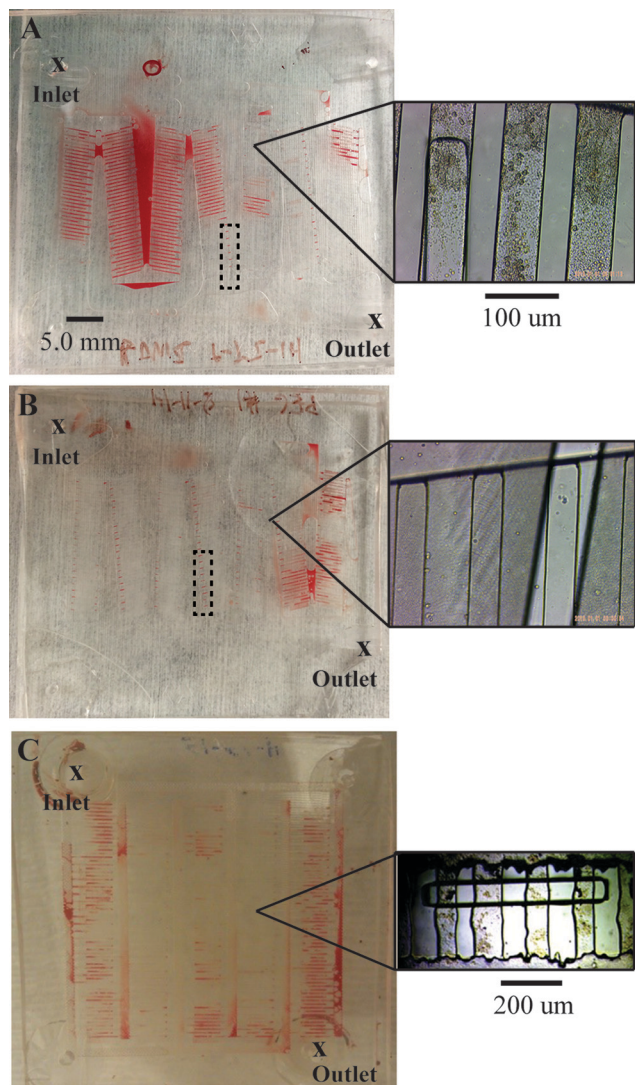
Fig. 9 Representative images of uncoated (A) and PEG-coated (B) lung devices following a PBS wash at the conclusion of the *in vitro* lifetime experiment. Image of an uncoated, washed lung device with old microchannel flow path from previous study[12] for reference (C). Surface-bound clots at the tips of the branching microchannels are highlighted with dashed boxes and 10× microscopic images of the capillaries are presented in the right insets. The dashed boxes are separate areas from the microscopic inset images, highlighting areas of low flow in the microchannel path.
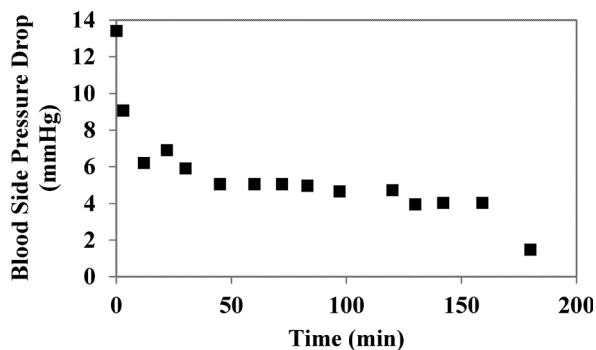

Fig. 10 Blood side pressure measurements over time for a PEG-coated lung device connected to the femoral vessels of an anesthetized rat (*n* = 1).
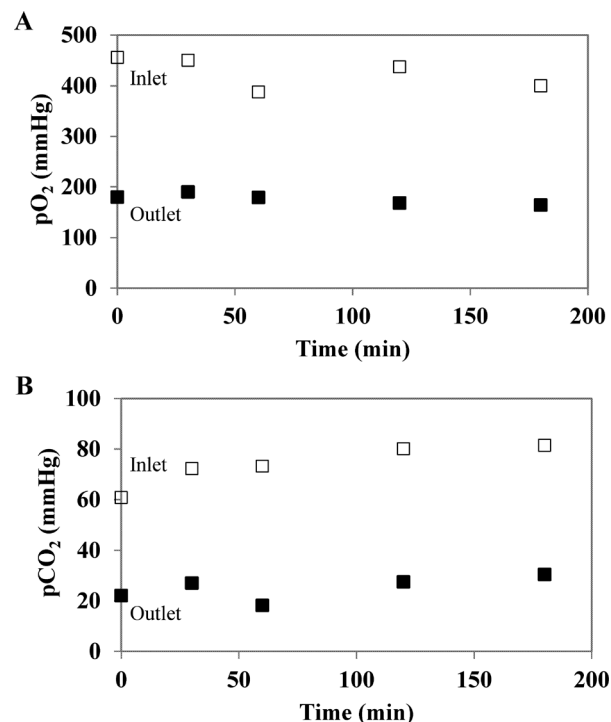

Fig. 11 Partial pressures of O_2 (A) and CO_2 (B) in the blood at the inlet (□) and outlet (■) of the rat-connected, PEG-coated artificial lung over the duration of the experiment (*n* = 1). Oxygen saturation, S_{O_2}, (not shown) remained at 100% at all time points because the rat was ventilated with pure oxygen while under anesthesia.

Discussion

Device design

The main advantages of the biomimetic flow path as designed (compared to our previous design[5,12]) are a more uniform distribution of shear stresses throughout the microchannel pathways and more efficient delivery of blood to the small diameter artificial capillaries. The bases for making these improvements have been well documented in previous literature, particularly the benefits of channel branching according to Murray's law.[16,20,21] More uniform shear and efficient delivery of blood are achieved through two main means: 1) microfluidic channels whose hydraulic diameter decreases as flow is diverted to smaller daughter vessels; and, 2) branching angles between parent and daughter vessels that are optimized to minimize the work required for blood flow. These concepts are demonstrated in Fig. 1. Although the effects on shear stress were not experimentally investigated, improvements in blood delivery efficiency is apparent from a lower pressure drop compared to our previous design.[5,12]

Pressure and gas exchange characterization

It is important to note that in Fig. 4 at the rated flow of 0.4 mL min^{-1}, the device is operating under a fluidic pressure of only 5–6 mmHg, well below the natural arterial pressure of a rat.[26] This feature makes it possible for blood to be driven

through the device entirely from the animal's natural arterio-venous (AV) pressure difference *in vivo* in peripheral AV (performed in this study) or pulmonary artery-left atrium configurations.[27] Other groups have also demonstrated the ability of properly designed artificial lungs to operate under natural pressure differences.[8,28–31]

The inverse blood flow-S_{O_2} relationship seen in Fig. 5A is most likely seen because as red blood cells increase their residence time in the capillary networks (lower flow rates), there is more time for gas diffusion to occur, increasing the saturation of hemoglobin sites with oxygen. The device's calculated rated flow fits well with the data in Fig. 5A, as the S_{O_2} remains at 100% before beginning to drop off between 0.4–0.6 mL min^{-1} of blood flow. The data in Fig. 5B and 6 are notable as they suggest that as long as our device is operated at or below the rated flow for blood, maximal gas exchange performance will be achieved for sweep gas flow rates greater than 1 mL min^{-1} (2× the rated blood flow). Maximal S_{O_2} is not reached in Fig. 5B due to the blood flow rate being slightly above the calculated rated flow; this was done to make changes in the blood saturation more apparent.

In vitro performance

Fig. 7 highlights the strong gas exchange performance of the PEG-coated lung device throughout the entire four hour lifetime experiment, significantly increasing oxygen saturation levels. These data represent first extended test of gas exchange over time for a microfluidic artificial lung. Because the devices are being operated slightly above the rated flow, maximal S_{O_2} will not be achieved. It is also important to note that S_{O_2} levels at all time points for the PEG-coated artificial lung are not statistically different. In comparison, oxygen saturation exiting the uncoated device significantly decreases after 60 min, and further decreases for the one device that lasted 120 min. It is theorized that this decrease in gas exchange performance is due to coagulation in the microchannel network, particularly in the capillary beds.[12] Clotting within the device would act to increase the effective oxygen diffusion distance between the blood and air or completely block blood flow within specific microchannels, thereby decreasing the effective area for gas exchange.

Evidence of the coagulatory response is also seen in Fig. 8. As blood clots accumulate within the microchannel network, they act to increase the fluidic resistance, and thus the pressure drop across the device.[12,13] At almost all time points the pressure across uncoated artificial lungs significantly exceeds that in PEG-coated devices. Furthermore, no uncoated device lasted longer than 150 minutes in this testing configuration, compared to every PEG-coated device completing the 240 minute experiment without failing. The consistent pressure drop across the PEG-coated device suggests that the intrinsic coagulatory response has not progressed nearly to the extent seen in the uncoated control. This is likely due in large part to the increase in the PDMS surface hydrophilicity provided by the PEG coating, resisting initial protein

adhesion and subsequent clot formation.[32–34] Although the circuit tubing used in this experiment was also hydrophobic in nature, the smallest tubing diameter was nearly 8× larger than the largest lung device channels, causing little concern for the potential confounding effects of clotting within the external circuit.

Finally, after washing the devices following the lifetime experiment, the difference in the coagulatory response between the two devices becomes clear (Fig. 9A and B). The uncoated device displays more extensive clotting throughout the microchannel network, as well as increased surface-bound fibrin and blood cell accumulation in the microscopic images. It is worth noting that in both devices, clotting is apparent at the tips of the first channel branches (dashed boxed areas in Fig. 9A and B). These areas were suspected to be "dead zones" in the channel design where stagnation of the blood could potentially take place, increasing the likelihood of clot formation.[35] These design features are required due to the alignment tolerance between the main and smaller channels, and because they are located at the distal ends of the channels, the clotting observed would not occlude blood flow through the rest of the device. Comparing the images in Fig. 9A and C, there appear to be more surface bound clots in the previous microchannel flow path (Fig. 9C) that did not adhere to Murray's law. This increase in clotting is especially apparent in the largest channels, where extensive yellowish-white fibrin deposits can be seen even where red blood cells are not present. It is in these largest channels that the first branches in the flow path occur, with high shear likely in this older design with 90° branching angles. However, definitive conclusions cannot be drawn between these two studies due to the different blood samples and anticoagulation protocols used.[12]

Taken together, these data present a clear link between coagulation as reflected in device lifetime and performance. This study represents the first extended *in vitro* blood evaluation of a microfluidic artificial lung, made possible through the application of a hemocompatible surface coating.

In vivo performance

The lifetime of the lung device attached to the rat's circulatory system (Fig. 10) reflects the trend seen in *in vitro* testing (Fig. 8). Once blood has filled and equilibrated within the device (~10 to 30 min), the measured pressure drop across the device remains stable until just before the end of the three hour experiment. This suggests that there is very little intrinsic coagulation occurring within and occluding the microchannel pathways. Upon further evaluation, it was determined that the sharp decrease in pressure observed at 180 min was due to a large clot that had developed in the circuit tubing leading to the inlet of the device. Clotting in the upstream circuit tubing would occlude blood flow into the device, artificially lowering the measured blood side pressure. This experimental issue, though confined to the tubing and not the device itself, dramatically impacted the success of

these experiments, causing us to end the protocol after $n = 1$. The tubing priming solution of heparin was the same 400 U kg^{-1} concentration as the injection, and was mixed directly into the blood volume of the rat. Although the combined total dose was larger than what is typical for patients undergoing cardiopulmonary bypass procedures,[36] it was deemed appropriate as no additional continuous heparin infusion would be administered throughout the experiment. However, given the half-life of heparin in the body at 400 U kg^{-1} to be 150 min,[37] it is possible that in the three hour duration of the experiment, the effects of this initial bolus dose may be wearing off near the conclusion when the tubing clotting was observed. Platelet counts were not measured in this experiment. However, we do not anticipate heparin-induced thrombocytopenia being a factor, as this condition is typically observed at least two days following heparin exposure, making it unlikely to play a significant role in this acute setting.[38]

Fig. 11 displays consistent gas exchange performance of the artificial lung throughout the experiment, further supporting a lack of clots forming on the capillary surfaces. As seen previously *in vitro* in uncoated devices (Fig. 7), gas exchange performance begins to fall quickly once the coagulation process begins. At first glance, it may appear strange that the device is reducing the p_{O_2} of the blood. However, due to the nature of the experimental setup, this is to be expected. Because the rat is ventilated with pure oxygen (98% after accounting for isoflurane) while under anesthesia, the partial pressure of the gas carried in the blood will be much higher than normal. As blood moves through the lung device, oxygen levels are equilibrated and lowered to those in the sweep gas (air), resulting in an outlet p_{O_2} of approximately 160 mmHg (21% of an atmospheric 760 mmHg). Similarly, the arterial blood enters the device with an elevated p_{CO_2} content of 60–80 mmHg due to the rat's suppressed respiration under anesthesia. The device acts to remove a significant amount of this dissolved carbon dioxide due to the low partial pressure of CO_2 in air. When the blood exits the artificial lung and is returned to the rat's circulation, the p_{CO_2} is slightly below the normal arterial range. These data suggest that the lung device is performing as expected as an AVCO2-R device given the experimental conditions and is able to successfully exchange blood gases to physiologically relevant levels without detriment to a living rat. It is important to note that the animal survived the surgical procedure and experiment and the measured vital signs[39] remained within normal ranges throughout the duration of the experiment. While one other group has performed *in vivo* testing of a microfluidic artificial lung,[40] these data represent the results of the first extended *in vivo* test.

Despite the success of this preliminary work, it should be noted that performing the femoral cannulation surgery in a rat model presented difficulties. The trauma of the surgical procedure and cannulation necessitated the use of a heparin injection to the animal in an attempt to reduce thromboembolisms and upstream clotting. Despite this effort, the tissue damage still may have played a role in activating the extrinsic coagulation cascade, contributing to the thrombosis observed within the circuit tubing. The results presented here are intended only as a preliminary proof of concept demonstration highlighting the ability of our device to function effectively in a rat model, not as a means to assert any statistically significant conclusions. Additional experiments were not performed due to the difficulties that we encountered with the surgical procedure, namely the cannulation of the femoral vessels. Thus we did not believe that more experiments could be justified with the low experimental success rate.

Conclusions

By constructing a microfluidic artificial lung featuring a biomimetic blood flow path and hemocompatible surface coating, we have significantly extended the functional lifetime of the device *in vitro*. Additionally, this lung device was successfully operated in a rat model to exchange O_2 and CO_2 at physiologically relevant levels. In order to build upon these results, construction methods for scaling up the device in order to increase the rated flow and test in larger animal models (rabbits, sheep) will be investigated. The use of a larger animal model and improved experimental setup will additionally allow for a more thorough *in vivo* evaluation of our device. Overall, the combination of microfabrication and surface coating techniques described here show promise as methods to improve the lifetime and functionality of many additional microfluidic blood-contacting devices.

Acknowledgements

Notes and references

1 K. Ota, *J. Artif. Organs*, 2010, **13**, 13–16.
2 T. Kniazeva, J. C. Hsiao, J. L. Charest and J. T. Borenstein, *Biomed. Microdevices*, 2010, **13**, 315–323.
3 K. A. Burgess, H.-H. Hu, W. R. Wagner and W. J. Federspiel, *Biomed. Microdevices*, 2008, **11**, 117–127.
4 J. A. Potkay, *Lab Chip*, 2014, **14**, 4122–4138.
5 J. A. Potkay, M. Magnetta, A. Vinson and B. Cmolik, *Lab Chip*, 2011, **11**, 2901–2909.
6 T. Kniazeva, A. A. Epshteyn, J. C. Hsiao, E. S. Kim, V. B. Kolachalama, J. L. Charest and J. T. Borenstein, *Lab Chip*, 2012, **12**, 1686–1695.
7 J. K. Lee, H. H. Kung and L. F. Mockros, *ASAIO J.*, 2008, **54**, 372–382.
8 D. M. Hoganson, H. I. Pryor, E. K. Bassett, I. D. Spool and J. P. Vacanti, *Lab Chip*, 2011, **11**, 700–707.

9   J. A. Potkay, *Biomed. Microdevices*, 2013, **15**, 397–406.

10 D. C. Duffy, J. C. McDonald, O. J. Schueller and G. M. Whitesides, *Anal. Chem.*, 1998, **70**, 4974–4984.

11 J. H. Elam and H. Nygren, *Biomaterials*, 1992, **13**, 3–8.

12 K. M. Kovach, J. R. Capadona, A. Sen Gupta and J. A. Potkay, *J. Biomed. Mater. Res., Part A*, 2014, **102**(12), 4195–4205.

13 Z. Zhang, J. Borenstein, L. Guiney, R. Miller, S. Sukavaneshvar and C. Loose, *Lab Chip*, 2013, **13**, 1963–1968.

14 S. Thorslund, J. Sanchez, R. Larsson, F. Nikolajeff and J. Bergquist, *Colloids Surf., B*, 2005, **45**, 76–81.

15 S. Lee and J. Vörös, *Langmuir*, 2005, **21**, 11957–11962.

16 T. Sherman, *J. Gen. Physiol.*, 1981, **78**, 431–453.

17 W. Federspiel and K. Henchir, in *Encyclopedia of Biomaterials and Biomedical Engineering*, ed. G. Bowlin and G. Wnek, Mercel Dekker, New York, 2004, pp. 910–921.

18 U. S. FDA, *Guidance for Cardiopulmonary Bypass Oxygenators 510(k) Submissions; Final Guidance for Industry and FDA Staff*, http://www.fda.gov/MedicalDevices/DeviceRegulationandGuidance/GuidanceDocuments/ucm073668.htm, Accessed 6/17/14, 2014.

19 A. Hill, *J. Physiol.*, 1910, **40**, 4–7.

20 C. Murray, *J. Gen. Physiol.*, 1926, **12**, 207–214.

21 C. Murray, *J. Gen. Physiol.*, 1926, **9**, 835–841.

22 J. E. Hall, *Guyton and Hall Textbook of Medical Physiology*, Saunders, Philadelphia, PA, USA, 2011.

23 A. M. Malek, S. L. Alper and S. Izumo, *JAMA*, 1999, **282**, 2035–2042.

24 S. Bhattacharya, A. Datta, J. M. Berg and S. Gangopadhyay, *J. Microelectromech. Syst.*, 2005, **14**, 590–597.

25 J. Deslauriers and J. Awad, *Ann. Thorac. Surg.*, 1997, **64**, 1581–1582.

26 Y. Wang, Y. Cong, J. Li, X. Li, B. Li and S. Qi, *PLoS One*, 2013, **8**, e60625.

27 R. W. Anderson and S. N. Vaslef, in *The Artificial Lung*, ed. R. W. Anderson and S. N. Vaslef, Eurekah.com/Landes Bioscience, Georgetown, TX, 2002, ch. 1, pp. 1–22.

28 W.-I. Wu, N. Rochow, E. Chan, G. Fusch, A. Manan, D. Nagpal, P. R. Selvaganapathy and C. Fusch, *Lab Chip*, 2013, **13**, 2641–2650.

29 T. Walles, *Expert Rev. Med. Devices*, 2007, **4**, 297–305.

30 M. Reng, A. Philipp, M. Kaiser, M. Pfeifer, S. Gruene and J. Schoelmerich, *Lancet*, 2000, **356**, 219–220.

31 J. Zwischenberger, C. Anderson, K. E. Cook, S. Lick, L. Mockros and R. Bartlett, *ASAIO J.*, 2001, **47**, 316–320.

32 W.-H. Kuo, M.-J. Wang, C.-W. Chang, T.-C. Wei, J.-Y. Lai, W.-B. Tsai and C. Lee, *J. Mater. Chem.*, 2012, **22**, 9991–9991.

33 H. Chen, L. Yuan, W. Song, Z. Wu and D. Li, *Prog. Polym. Sci.*, 2008, **33**, 1059–1087.

34 M. B. Gorbet and M. V. Sefton, *Biomaterials*, 2004, **25**, 5681–5703.

35 C. Esmon, *Blood Rev.*, 2009, **23**, 225–229.

36 N. Guzzetta, B. Miller, K. Todd, F. Szlam, R. Moore and S. Tosone, *Anesth. Analg.*, 2005, **100**, 1276–1282.

37 J. Hirsh, S. S. Anand, J. L. Halperin and V. Fuster, *Circulation*, 2001, **103**, 2994–3018.

38 G. Lee and G. Arepally, *Hematol. Oncol. Clin. North Am.*, 2013, **27**, 541–563.

39 S. L. Sciences, Anesthetized and Surgical Monitoring with MouseOx® Plus, http://www.starrlifesciences.com/surgical-monitoring, Accessed 9/8/14, 2014.

40 N. Rochow, A. Manan, W.-I. Wu, G. Fusch, S. Monkman, J. Leung, E. Chan, D. Nagpal, D. Predescu, J. Brash, P. R. Selvaganapathy and C. Fusch, *Artif. Organs*, 2014, **38**(10), 856–866.